Thin-film composite forward osmosis membranes functionalized with graphene oxide–silver nanocomposites for biofouling control

Journal of Membrane Science

Revised: September 9, 2016

Andreia F. Faria[1], Caihong Liu[1,2], Ming Xie[1,3], Francois Perreault[1,4], Long D. Nghiem[5], Jun Ma[2], and Menachem Elimelech [1*]

[1]*Department of Chemical and Environmental Engineering, Yale University, New Haven, Connecticut 06520-8286, USA*

[2] *State Key Laboratory of Urban Water Resource and Environment, Harbin Institute of Technology, Harbin 150090, China*

[3]*Institute for Sustainability and Innovation, College of Engineering and Science, Victoria University, PO Box 14428, Melbourne, Victoria 8001, Australia*

[4]*School of Sustainable Engineering and the Built Environment, Arizona State University, Tempe, AZ, 85287-3005.*

[5] *Water Infrastructure Laboratory, School of Civil, Mining and Environmental Engineering, University of Wollongong, Wollongong, NSW 2522, Australia*

* Corresponding author: Menachem Elimelech, Email: menachem.elimelech@yale.edu, Phone: (203) 432-2789

ABSTRACT

Innovative approaches to prevent bacterial attachment and biofilm growth on membranes are critically needed to avoid decreasing membrane performance due to biofouling. In this study, we propose the fabrication of anti-biofouling thin-film composite membranes functionalized with graphene oxide–silver nanocomposites. In our membrane modification strategy, carboxyl groups on the graphene oxide–silver nanosheets are covalently bonded to carboxyl groups on the surface of thin-film composite membranes via a crosslinking reaction. Further characterization, such as scanning electron microscopy and Raman spectroscopy, revealed the immobilization of graphene oxide–silver nanocomposites on the membrane surface. Graphene oxide–silver modified membranes exhibited an 80% inactivation rate against attached *Pseudomonas aeruginosa* cells. In addition to a static antimicrobial assay, our study also provides insights on the anti-biofouling property of forward osmosis membranes during dynamic operation in a cross-flow test cell. Functionalization with graphene oxide–silver nanocomposites resulted in a promising anti-biofouling property without sacrificing the membrane intrinsic transport properties. Our results demonstrated that the use of graphene oxide–silver nanocomposites is a feasible and attractive approach for the development of anti-biofouling thin-film composite membranes.

Keywords: forward osmosis, thin-film composite membranes, graphene oxide, silver nanoparticles, antimicrobial activity, biofouling control.

1. Introduction

Global demand for drinking water is expected to increase in the coming decades due to rapid population growth and climate change [1]. Membrane-based water purification processes play a crucial role in mitigating water scarcity worldwide [1, 2]. Due to their high permeate water flux and salt rejection capabilities, thin-film composite (TFC) membranes have been considered the state-of-the art for water desalination technologies such as reverse osmosis (RO) and forward osmosis (FO) [1-4]. Despite these advantages, TFC membranes encounter several operational limitations. One significant challenge is the attachment of microorganisms and subsequent biofilm formation [5, 6].

The growth of bacteria as biofilms can affect membrane performance by decreasing permeate water flux and salt rejection [6]. Furthermore, biofouling development can lead to an increase in energy consumption [5-7]. Ordinary procedures such as pretreatment and chemical cleaning are being used to mitigate biofouling [5, 6]. However, no pre-treatment can completely eliminate biofouling, and it is well known that the polyamide layer of TFC membranes undergoes degradation in the presence of chemical oxidants such as chlorine [8]. Therefore, there is a critical need to develop innovative strategies to control microbial proliferation at the membrane surface.

Several studies have proposed to modify the surface of TFC membranes with polymers [9], bio-active molecules [10], or antimicrobial nanomaterials [11] in order to impart antimicrobial activity and biofouling resistance to the membrane. For instance, it has been shown that TFC membranes functionalized with silver or copper nanoparticles presented a diminished susceptibility to biofouling [12, 13]. Alternatively, carbon-based nanomaterials such as carbon nanotubes (CNTs) and graphene oxide (GO) have also been linked to the polyamide layer to generate TFC membranes with enhanced antimicrobial properties [14-16].

Antimicrobial nanomaterials can be incorporated by embedding them within the membrane polymeric matrix [17]. Post-fabrication modification, on the other hand, is focused on the immobilization of nanomaterials at the membrane surface via physical interactions [13], chemical binding [16], or layer-by-layer techniques [18]. Because the nanomaterials are placed specifically at the membrane surface, post-fabrication functionalization is unlikely to affect significantly the properties of the polyamide layer [15, 16]. This technique is also material-and

cost-efficient since fewer nanomaterials are required to tailor the membrane surface chemistry [15, 16].

Since the first discovery of the electronic properties of pristine graphene sheets [19], researchers have joined efforts to unveil the properties and potential applications of graphene-related materials. Graphene oxide, produced from the chemical exfoliation of graphite, comprises a layer one atom-thick of graphene functionalized with oxygen atoms [20]. The vast majority of GO applications have been driven by their scalable and low cost production, high stability in water, large surface area, and abundance of oxygen-containing functional groups [21, 22].

Owing to these chemical functionalities, GO can be easily combined with a wide variety of polymers and nanoparticles. Using the GO surface to anchor silver nanoparticles appears promising, especially due to the surface functional groups that serve as nucleation points for particle growth [23, 24]. As the formation of silver nanoparticles (AgNPs) occurs in a one-pot in-situ reaction, GO sheets work as a high surface area template for particle attachment and the use of a capping agent is not required. In addition to the presence of AgNPs themselves, graphene oxide–silver nanocomposites (GOAg) offer a diverse and inherent presence of oxygen-containing functional groups (e.g., ketones, hydroxyl, carbonyl, and carboxyl) that are important to bind graphene sheets to the surface of a wide range of materials [25]. For antimicrobial purposes, GOAg sheets can simultaneously inactivate bacterial cells through release of silver ions while providing a large surface area for contact with microbial cells [23, 25]. These properties are highly relevant in fabricating antimicrobial surfaces through chemical modification of polymeric materials with nanomaterials.

In this study, we demonstrate, for the first time, an innovative approach to modify TFC membranes with GOAg nanocomposites and the associated effects on mitigating biofouling. In addition to conventional antibacterial properties, we offer a step toward understanding how biofilm formation on TFC membranes is influenced by the presence of GOAg nanocomposites. Chemical modification with GOAg sheets led to a strong antimicrobial activity and the resulting TFC-GOAg membranes efficiently suppressed biofilm formation under cross-flow test conditions. Our results demonstrate that GO-based nanocomposites can serve as building blocks to fabricate membranes with advanced properties for water separation processes.

2. Materials and Methods

2.1 Materials and Chemicals

Graphite powder SP-1 was obtained from Bay Carbon (Bay City, MI, USA). Sulfuric acid (H_2SO_4, 95.0%), hydrogen peroxide (H_2O_2, 30.0%), sodium chloride (NaCl crystals), and sucrose were purchased from J. T. Baker (Phillipsburg, NJ, USA). Potassium persulfate ($K_2S_2O_8$, 99.0%), phosphorous pentoxide (P_2O_5, 98.0%), potassium permanganate ($KMnO_4$, 99.0%), hydrochloric acid (HCl, 37.0%), silver nitrate ($AgNO_3$, 99%), dextrose ($C_6H_{12}O_6$, 99%), ammonium hydroxide (NH_4OH, 30%), ammonium chloride (NH_4Cl, 99%), potassium phosphate monobasic (KH_2PO_4, 99%), calcium chloride hydrate ($CaCl_2.H_2O$, 99%), sodium bicarbonate ($NaHCO_3$, 99%), magnesium sulfate heptahydrate ($MgSO_4.7H_2O$, 98%), MES monohydrate (99%), HEPES buffer (99%), 1-ethyl-3-(3-dimethylaminopropyl) carbodiimide hydrochloride (EDC, 98%), N-hydroxysuccinimide (NHS, 98%), ethanol (anhydrous, 99,5%), 3-[(3-cholamidopropyl)-dimethylammonio]-1-propane sulfonate (CHAPS, 98%), dithiothreitol (DTT, 98%), and paraformaldehyde (95%) were purchased from Sigma-Aldrich (St. Louis, Missouri, USA). Trichloro-1, 2, 2-trifluoroethane (Freon, 99%) was purchased from America Refrigerants (Sarasota, FL, USA). Luria-broth medium for bacteria cultivation was purchased from Becton, Dickinson and Company (Sparks, MD, USA). Glutaraldehyde solution (50%) was acquired from Amresco (Solon, OH, USA). Sodium cacodylate buffer (pH 7.4) was acquired from Electron Microscopy Sciences (Hatfield, PA, USA). Polyamide thin-film composite (TFC) forward osmosis membranes were obtained from HTI (Hydration Technology Innovation) (Albany, OR, USA) and stored in deionized (DI) water at 4°C prior to use. DI water was supplied by a Millipore System (Millipore Co., Billerica, MA, USA).

2.2 Graphene oxide and graphene oxide–silver (GOAg) synthesis

GO was synthesized using a modified Hummers and Offemans' method [26], and its details have been provided in previous publications [25, 27, 28]. Succinctly, a graphite sample was subjected to two consecutive oxidation processes. First, graphite powder (1.0 g) was placed in H_2SO_4 (5 mL) and pre-oxidized in the presence of $K_2S_2O_8$ (1.0 g) and P_2O_5 (1.0 g) at 80°C for 4.5 hours. Then, the resulting black solid (pre-oxidized) was placed into H_2SO_4 (40 mL) and reacted with $KMnO_4$ (5.0 g) at 35°C for 2.5 hours. After the oxidation reaction, DI water (77.0 mL) was introduced into the suspension and the mixture was left to react for an additional two hours at room temperature. To complete the oxidation, H_2O_2 (30%) (5 mL) was added to the dispersion and the formation of a brilliant yellow color was observed. The dispersion was left to rest for two days, and the precipitate was recovered by centrifugation (12,000 x *g*, 4 °C,

for 20 minutes). The resulting material was washed with HCl (10% v/v) and DI water to remove any traces of chemicals. The graphite oxide was resuspended in DI water and additionally purified by dialysis (3,500 Da membranes, Spectrum Laboratories, Inc., CA, USA) for three or four days. The final brown suspension was frozen in liquid nitrogen, dried by lyophilization, and stored at room temperature.

GOAg nanocomposites were synthesized by employing Tollens' modified method, which is based on the complexation of Ag^{+} ions with NH_4OH and further reduction using saccharides [29]. To prepare GOAg nanocomposites, GO (12.5 mg) was dispersed in DI water (35 mL) and bath-sonicated (Aquasonic Model 150T) for 30 minutes. $AgNO_3$ (8.65 mg) was dissolved in 5 mL of DI water and then combined with a 50 mM NH_4OH solution (5 mL). The resulting solution was stirred for 10 minutes. Then, the silver solution was introduced to the prior GO dispersion and the mixture was bath-sonicated for an additional 20 minutes. Immediately after sonication, 5 mL of a glucose solution (100 mM) was added by drops. The reaction was conducted overnight at room temperature. After synthesis completion, the color of the suspension changed from brown to green-blue, indicating the nanocomposite formation. To remove the excess of chemical residues, the GOAg nanocomposite suspension was purified by dialysis (3,500 Da membranes, Spectrum Laboratories, CA, USA) for three hours and further dried by lyophilization.

GOAg nanocomposites were characterized by UV-Vis spectroscopy (Hewlett Packard 8453 spectrophotometer) through the detection of the plasmon absorption band. To evaluate the content of silver in the GOAg sample, thermogravimetric analysis (TGA) was carried out using a Setaram Setsys 1750 TG-DTA. The thermogravimetric curves were obtained from 100 to 800°C at a heating rate of 5°C min^{-1} under synthetic air. The morphological properties of GO and GOAg nanocomposites were investigated by transmission electron microscopy (TEM) at an accelerating voltage of 200 kV (FEI Tecnai Osiris).

2.3 Functionalization of TFC membranes with GO and GOAg nanocomposites

The polyamide active layer of thin-film composite (TFC) membranes was functionalized with GO or GOAg using a well-stablished method adapted from previous studies [15, 16]. Pristine TFC membranes were placed in frames and sealed with clips to avoid any leakage. With only the active (top) surface exposed, the membranes were kept on an orbital shaker at 60 rpm at room temperature throughout the functionalization procedure.

GO and GOAg nanocomposites were chemically bound to the TFC membranes using EDC and NHS as crosslinks. The entire functionalization process can be divided into three steps. The first step is the activation of the native carboxylic functional groups on TFC membranes. For this, EDC (4.0 mM) and NHS (10.0 mM) were dissolved in 10 mM MES buffer (pH 5.0) and left to react with the membrane surface for two hours. Next, the solution was removed and the membrane surface was rinsed twice with DI water. In the presence of EDC and NHS, the native carboxyl functionalities on the membrane surface were converted to reactive ester groups. In the second step, the activated carboxyl groups were reacted with ethylene diamine (ED) (10 mM) in a 0.15 M NaCl and 10 mM HEPES buffer (pH 7.5) for one hour to yield an amine-terminated membrane surface. The membrane surface was then rinsed twice with DI to remove unbound ED.

The third step comprises the activation of the carboxylate groups on GO and GOAg by EDC and NHS, as described earlier for the pristine TFC membrane. Twenty-five milliliters of the GO and GOAg dispersions (250 μg mL^{-1}) were diluted with 20 mL of 10 mM MES buffer (pH 6). EDC (1.5 mM) and NHS (2.5 mM) were dissolved in 5 mL of MES buffer (pH 6.1) and slowly poured into the GO and GOAg dispersions. The system was kept stirring for 30 minutes at room temperature. EDC and NHS decreased the buffer pH to 5.5-5.8. Before contact with the membrane surface, pH was adjusted to 7.2 using a sodium hydroxide solution (1 M). After activation, the ED-functionalized membrane coupons were brought into contact with 20 mL of the activated GO and GOAg samples, and the system was gently stirred at room temperature for three hours. The intermediate reactive esters on GO and GOAg react with the primary amine functional groups, thus irreversibly binding the nanomaterials to the membrane surface. At the end of the reaction, the membranes were rinsed to wash out the unbound materials and restore the unreacted carboxyl groups. The TFC membranes modified with GO or GOAg are referred to as TFC-GO and TFC-GOAg, respectively.

2.4 Membrane characterization

The presence of GO and GOAg nanocomposites on the membrane surface was confirmed by scanning electron microscopy (SEM) using an XL-Philips scanning electron microscope. A Cressington (208 carbon) sputtering machine was applied to coat the sample with a thin layer (10-20 nm) of carbon. Images were taken at an acceleration voltage of 10 kV. Energy dispersive spectroscopy (EDS) was utilized to detect the presence of silver. Raman spectroscopy (Horiba Jobin Yvon HR-800) was also used to characterize the functionalization of TFC membranes

with GO or GOAg. At least five random locations on the membrane surface were scanned and the Raman spectra were recorded utilizing a 532 nm laser excitation.

Surface hydrophilicity was investigated through static contact angles (Theta Lite Optical Tensiometer TL100). Considering the intrinsic variability of this technique, eight measurements were taken at random spots on several dried membrane coupons. Membrane surface roughness was analyzed by atomic force microscopy (AFM, Bruker, Digital Instruments, Santa Barbara, CA, USA) in a peak force tapping mode. Scanasyst-air silicon tips, coated with reflective aluminum, were employed (Bruker Nano, Inc., Camarillo, CA, USA). The tip has a spring constant of 0.4 N m^{-1}, resonance frequency of 70 kHz, tip radius of 2 nm, and cantilever length of 115 μm and width of 25 μm. All images were captured from six randomly selected areas on each membrane coupon. The average surface roughness was calculated from three different measurements for each membrane sample (pristine and modified).

The transport properties of the membrane were determined in a cross-flow FO filtration system according to a four-step method reported in our previous publication [30]. Briefly, the experiments were carried out in a laboratory-scale cross-flow forward osmosis unit. Speed gear pumps (Cole-Parmer, Vernon Hills, IL, USA) were used to circulate the solutions in a cross-flow velocity of 9.56 cm s^{-1}. DI water and NaCl solutions were used as feed and draw solutions, respectively. A water bath (Neslab, Newington, NH, USA) was applied to keep the temperature of both feed and draw solutions constant at 25 ± 0.5°C. Water flux was determined by monitoring the rate of change in weight of the draw solution. NaCl concentration in the feed solution was measured at regular intervals using a conductivity meter (Oakton Instruments, Vernon Hills, IL, USA) in order to quantify the reverse NaCl flux. Four different stages were employed by changing the NaCl concentrations of the draw solution. These measurements allowed for the determination of the water permeability coefficient (A), the salt permeability coefficient (B), and the membrane structural parameter (S). These parameters were adjusted to fit the experimental data of water and reverse salt fluxes to the corresponding governing equations.

2.5 Assessing antimicrobial activity of functionalized TFC membranes

Pseudomonas aeruginosa (ATCC 27853) was used as the model bacteria. *P. aeruginosa* cells were cultivated on Lauria-Bertani (LB) broth overnight at 37°C. The bacterial cells were then diluted (1:50) in fresh LB medium until they reached an optical density of 1.0 at 600 nm (OD_{600nm}) (~2 hours), which corresponds to a concentration of ~10^9 CFU mL^{-1}. The bacterial

suspension was then washed twice with saline solution (0.9%) by centrifugation for 2 minutes at 10,000 rpm to remove the excess growth medium constituents. The resulting suspension was diluted to 10^8 CFU mL^{-1} in a sterile isotonic solution (NaCl, 0.9% w/v).

A plate-counting method was employed to evaluate the inactivation of bacteria by the GO and GOAg functionalized membranes. TFC, TFC-GO, and TFC-GOAg membranes were cut in round coupons of approximately 1.5 cm^2 and placed on plastic holders. These plastic holders only allowed the membrane top surface to contact the bacterial suspension. The membrane surface was in contact with the bacterial solution (2 mL) for three hours at room temperature. The bacterial suspension was then discarded and coupons were rinsed with sterile 0.9% saline solution to remove the non-adhered bacteria. The membrane coupons were transferred to 50 mL falcon tubes containing 10 mL 0.9% saline solution. Subsequently, the falcon tubes were bath-sonicated (26 W L^{-1}, FS60 Ultrasonic Cleaner) for 15 minutes to detach the bacterial cells from the membrane surface. Aliquots were collected, sequentially diluted in 0.9% saline solution, and spread on LB agar plates. Plates were incubated overnight at 37°C.

The morphology of the attached cells was imaged by SEM. The bacteria cells attached to the membrane coupons were fixed using Karnovsky's solution (4% paraformaldehyde and 5% glutaraldehyde diluted in 0.2 M cacodylate buffer pH 7.4) for three hours. The cells were consecutively dehydrated by immersing the membrane coupons in water-ethanol (50:50, 30:70, 20:80, 10:90, and 100% ethanol) and ethanol-freon solutions (50:50, 25:75, and 100% freon) for 10 minutes. After the sequential dehydration steps, the fiber coupons were dried overnight in a desiccator at room temperature. The samples were then sputter-coated with 10 nm carbon (Cressington coater, 208 carbon), and the bacteria cells were imaged by SEM (XL series-Philips) operating at an acceleration voltage of 10 kV.

2.6 Membrane biofouling and biofilm characterization protocols

Biofilm development was evaluated for the pristine TFC, TFC-GO, and TFC-GOAg membranes in a custom-designed cross-flow test cell. *P. aeruginosa* was cultivated as described above and then transferred to a synthetic wastewater composed of 1.2 mM sodium citrate, 0.8 mM NH_4Cl, 0.2 mM KH_2PO_4, 0.2 mM $CaCl_2 \cdot H_2O$, 0.5 mM $NaHCO_3$, 8.0 mM NaCl, and 0.15 mM $MgSO_4 \cdot 7H_2O$, as previously reported [31]. The initial bacteria concentration in the synthetic wastewater solution was 10^7 cells mL^{-1}. The temperature was kept at 25°C throughout the experiment.

At the end of the experiment, the membrane coupons were cut in small pieces (1 cm^2) and placed in individual petri dishes. The samples were rinsed with a 0.9% NaCl solution to remove non-adhered bacteria, and the biofilm was stained with SYTO 9 and propidium iodide (PI) (Live/Dead® BacLight™, Invitrogen, USA). Live and dead cells were stained in green and red, respectively. Concanavalin A (Con A, Alexa Flour® 633, Invitrogen, USA) was used to stain exopolysaccharides (EPS) in blue. The dyes were in contact with the biofilm for at least 20 minutes in the absence of light. Samples were rinsed to remove the excess stain and imaged using a confocal laser scanning microscopy (Zeiss LSM 510, Carl Zeiss, Inc.). Lasers at the wavelength of 488 nm (argon), 561 nm (diode-pumped solid state), and 633 nm (helium–neon) were used to excite SYTO 9, PI, and Con A staining, respectively. Random locations were scanned to obtain representative areas of the biofilm. Intrinsic characteristics such as biofilm thickness and biovolume of live and dead bacterial components of the biofilm were also determined.

Biofilm total organic carbon (TOC) and protein concentration were also quantified. For TOC measurements, membrane sub-sections (2 cm × 2 cm) were re-suspended in 24 mL sterile wastewater with 10 µL of 1 M HCl. Samples were then sonicated on ice in three 30-second cycles to remove organic content from the membrane. TOC in the resultant solution was then analyzed using a TOC analyzer (TOC-V, Shimadzu, Japan). TOC concentrations were normalized by membrane sample area. For protein quantification, membrane sub-sections (2 cm × 2 cm) were cut and suspended in 2 mL Eppendorf tubes with 1 mL 1X Lauber buffer (50 mM HEPES (pH 7.3), 100 mM NaCl, 10% sucrose, 0.1% CHAPS, and 10 mM DTT) and probe sonicated on ice (three 30-second cycles) using an ultra-cell disruptor. The membrane was then removed and cell extracts were centrifuged at 12,000 rpm for 10 minutes to remove detritus matter. The supernatant was then collected for protein quantification using a BCA protein assay kit (Thermo Scientific, IL).

3. Results and Discussion

3.1 Physicochemical characteristics of GO and GOAg nanocomposites

The chemical exfoliation of graphite produces a brown dispersion composed of single-layer graphene oxide (GO) sheets (**Figure 1A**). A typical GO sample characteristically has a wide size distribution. GO average size is dependent on several factors such as time of reaction, the graphite precursor, and the concentration and type of oxidizing agent used during sample preparation. The SEM image of an aqueous suspension of our prepared GO (**Figure 2**) shows the presence of flat sheets with an average area of 0.36 ± 0.37 μm^2. The average size of GO

sheets has been shown to influence their reactivity, in particular the cytotoxicity to bacterial cells [28, 32].

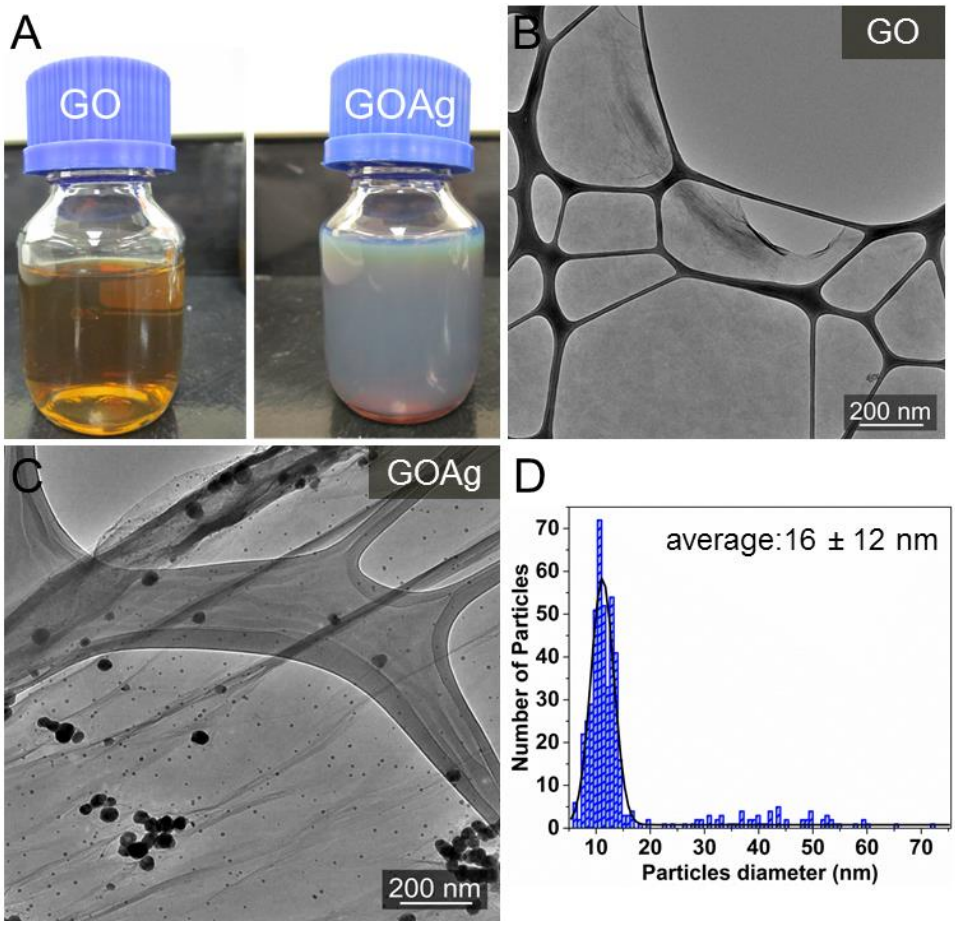

Figure 1: (A) Photographs of bare GO (left) and GOAg nanocomposites (right) dispersions. The green-blue color is an indicator of the formation of silver nanoparticles on GO surface. GOAg nanocomposites were prepared through in-situ reduction of $AgNO_3$ (1 mM) in the presence of GO sheets (125 µg mL^{-1}). Representative transmission electron microscopy (TEM) images of (B) GO and (C) GOAg nanocomposites. (D) size distribution of silver nanoparticles attached to GO surface. Silver nanoparticles revealed an average size of 16 ± 12 nm after counting approximately 200 particles on several TEM images.

For the preparation of GOAg nanocomposites, GO powder was dispersed in DI water and mixed with the precursor $AgNO_3$. The reaction was conducted at alkaline conditions due to the addition of ammonium hydroxide (NH_4OH); glucose (dextrose) was used as a reducing agent. The change in color from brown to green-blue was an indicator of the decoration of GO sheets with AgNPs (**Figure 1A**). Previous studies have reported the use of sugar to reduce Ag^+ ions to silver nanoparticles [29]. This method is widely known as the *Tollens* reaction. The mechanism involves the interaction of Ag^+ ions with NH_4OH to form intermediate species

$(Ag(NH_3)_2)^+$ that are then reduced to nanoclusters upon contact with the sugar molecules [33]. It is worth mentioning that the reducing property of monosaccharides, such as glucose, is attributable to the presence of free aldehyde or ketone functional groups on the sugar molecules. In comparison to many of the processes already reported in the literature, the *Tollens* method is advantageous since it applies a non-toxic and an environmental friendly molecule as a reducing agent. Moreover, the chemical reaction does not require high temperatures or the use of aggressive organic solvents [23, 24, 34, 35].

Given the change in color, a UV-Vis spectrum was recorded to indirectly confirm the formation of silver nanoparticles in the GO dispersion. The plasmon band (~ 440 nm) on the UV-Vis spectrum of GOAg nanocomposites suggests the presence of nanoparticles in the GO dispersion (**Figure S1A**) [23, 25]. The additional absorption peaks at approximately 230 and 305 nm are associated with π-π^* transitions of C-C aromatic and n-π^* transitions of C=O bonds of GO sheets, respectively [23, 35, 36]. X-ray diffraction (XRD) analyses have also been applied as a way to demonstrate the crystallographic features of the silver nanoparticles deposited on GO sheets. For GOAg nanocomposites, the X-ray diffraction spectrum (**Figure S1B**) displays peaks at 38.3, 44.3, 64.4, and 77.3° that correspond to the 111, 200, 220, and 311 crystalline planes of AgNPs, respectively [36]. Thermogravimetric analysis was carried out to investigate the thermal decomposition pattern of both GO and GOAg (**Figure S1C**). TGA curves also provide information about the silver content in the GOAg sample [23, 24]. The residues above 600°C indicate that the relative content of silver is approximately 10 wt % of the total GOAg nanocomposites (**Figure S1C**).

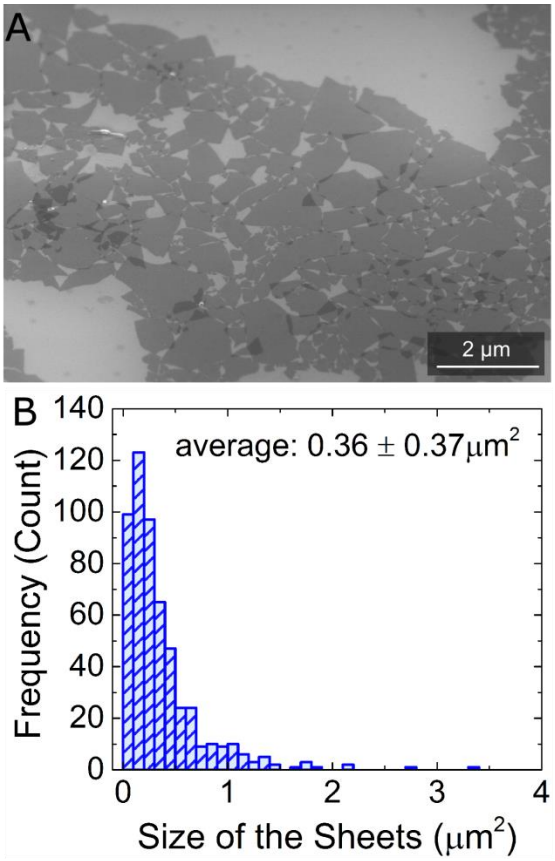

Figure 2: (A) Scanning electron microscopy (SEM) image of graphene oxide (GO) sheets. Graphene oxide dispersion was deposited on a silicon wafer and the images were taken at an acceleration voltage of 15 kV. (B) size distribution of GO sheets; the average size was estimated by measuring the area (μm^2) of multiple GO sheets using the software ImageJ.

The decoration of GO sheets with AgNPs was confirmed by transmission electron microscopy (TEM), as shown in **Figure 1C**. The AgNPs appeared as black dots distributed throughout the graphene surface with an average size of 16 ± 12 nm (**Figure 1D**). Both GO and GOAg nanocomposites showed a wrinkled and paper-like morphology on the TEM images (**Figures 1B and C**). Since particles were not found detached from GO sheets, we surmise the nucleation occurs preferentially on the graphene surface. The negatively charged oxygen-containing functional groups on GO likely offer nucleation sites for the Ag^+ ions via electrostatic interaction [23, 35]. Once adsorbed on GO sheets, Ag^+ ions can be reduced to Ag^0 nanoparticles in the presence of a reducing agent. The physicochemical characteristics of GOAg nanocomposites may differ depending on the degree of oxidation of GO sheets and the initial concentration of silver utilized [37, 38].

3.2 GO and GOAg sheets are covalently bound to the membrane surface

The binding of GO and GOAg nanocomposites to TFC membranes was developed through a reaction mediated by EDC and NHS. The polyamide layer of TFC membranes possesses native carboxyl groups that can react with ethylene diamine (ED) via EDC and NHS to yield an amine-terminated surface. Similarly, the carboxyl groups on GO layer are activated when exposed to EDC and NHS in a buffered solution. During this activation, the carboxyl groups on GO are converted to intermediate esters that readily react with amine groups on ED-functionalized TFC membranes. GO and GOAg sheets are covalently linked to the polyamide layer through the formation of an amide bond between carboxyl groups of GO and the amine groups on ED-functionalized TFC membranes. A scheme in **Figure 3** illustrates the reaction mechanism involved in the binding of GOAg sheets to the membrane surface.

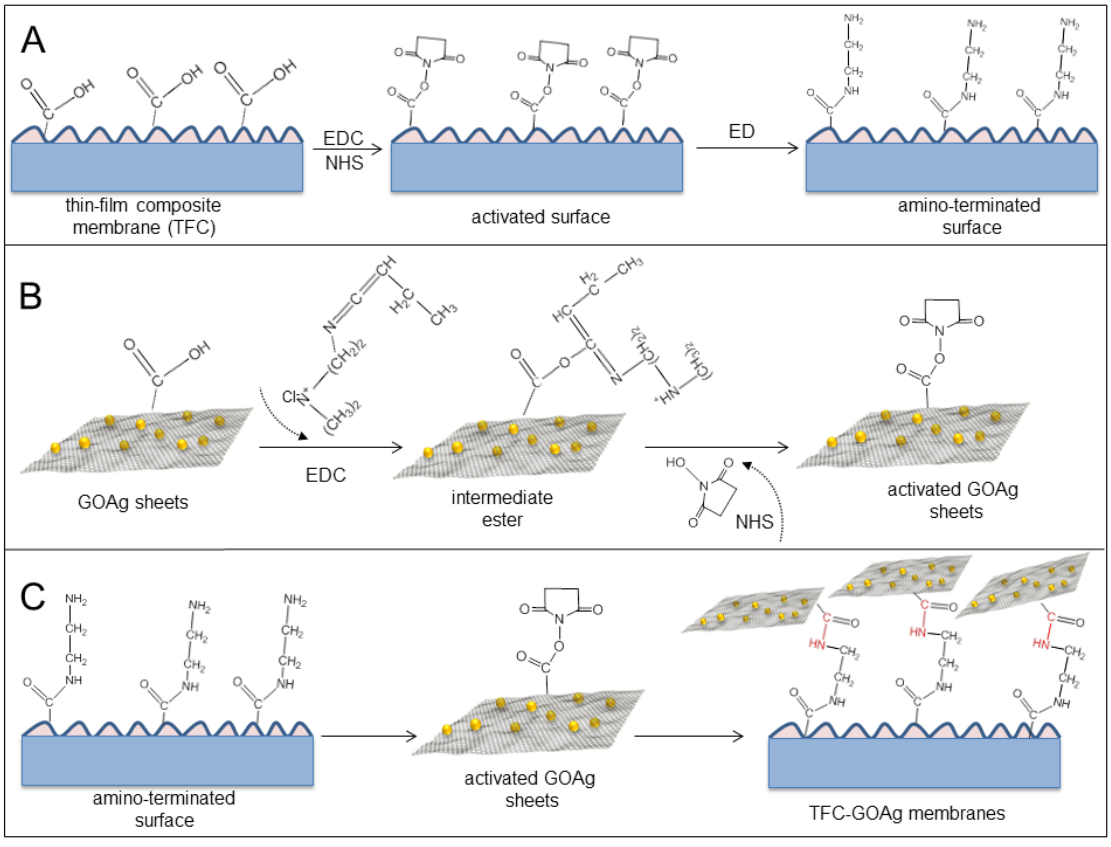

Figure 3: Scheme illustrating the three-sequential steps (A, B, and C) for binding GOAg sheets to the surface of thin-film composite membranes. (A) Carboxylic groups on the polyamide layer are converted into primary amine groups; the native carboxylic groups are activated by EDC and NHS to generate a highly reactive ester that spontaneously reacts with ethylenediamine (ED) to allow an amine-terminated surface. (B) Carboxylic functional groups on GOAg sheets are activated in presence of EDC and NHS. (C) The amine-terminated TFC membrane contacts the activated GOAg sheets. This reaction leads to the binding of graphene sheets through the formation of an amide bond.

SEM imaging of the pristine membrane surface shows a ridge-and-valley morphology characteristic TFC membrane (**Figure 4A**) [13, 15, 16]. The areas where the polyamide layer was modified with GO or GOAg sheets appeared as dark spots on the membrane surface (**Figures 4B and C)**. No such dark spots are present on the SEM images of pristine membranes (**Figure 4A**). The rough surface of the polyamide layer seems to be covered by GO or GOAg nanosheets and small bright features (~50 nm) were detected on the surface of TFC-GOAg membranes (**Figure 4C**). Energy dispersive spectroscopy (EDS) spectrum acquired directly from those bright spots revealed a peak at 4.0 keV that is attributable to silver (**Figure 4D**). A visual inspection indicated that TFC membranes did not present drastic changes in color after binding GO or GOAg nanocomposites.

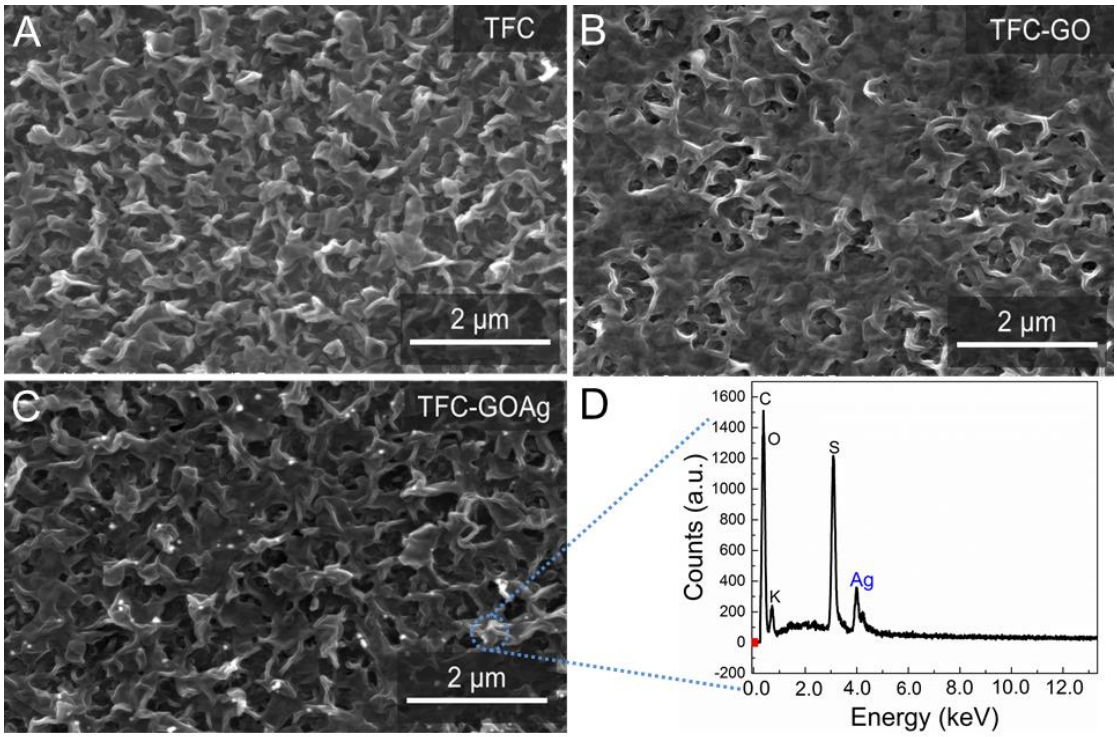

Figure 4: Scanning electron microscopy (SEM) images of the polyamide active layer of (A) pristine TFC, (B) TFC-GO, and (C) TFC-GOAg membranes. Images were taken at an acceleration voltage of 10 kV. (D) Energy dispersive spectroscopy (EDS) spectrum of bright dots on the surface of TFC membranes modified with GOAg. The peak at 4.0 keV is commonly ascribed to the presence of silver.

In addition to SEM imaging, GO and GOAg-modified membranes were characterized by Raman spectroscopy (**Figure 5**). The functionalization of TFC membranes with both nanomaterials was indirectly confirmed through changes in the intensity ratio between the peaks at 1148 and 1620 cm^{-1} (I_{1148}/I_{1620}), as reported in our previous publication [16]. Among several absorption peaks, Raman spectrum of TFC membranes is particularly characterized by

the presence of symmetric C-O-C stretching (~1148 cm^{-1}) and phenyl ring vibration (~1590-1620 cm^{-1}) [39]. It is already well known that bare GO displays two reference peaks at 1350 cm^{-1} (D band) and 1590 cm^{-1} (G band) in the Raman spectrum [40]. With the binding of GO and GOAg nanocomposites, the intensity of the peak at 1148 cm^{-1} is expected to decrease, whereas the intensity of the peak at 1620 cm^{-1} is likely to increase due to the contribution of the G band from GO sheets. Comparison of multiple functionalized membranes demonstrated that the I_{1148}/I_{1620} ratio for TFC-GO (0.30 ± 0.12) and TFC-GOAg (0.26 ± 0.12) was significantly decreased ($p < 0.005$) in comparison to pristine TFC membranes (0.93 ± 0.20) (**Figure 5**). The noticeable decrease in the I_{1148}/I_{1620} ratio is an additional confirmation of the successful functionalization of TFC membranes with GO or GOAg nanosheets.

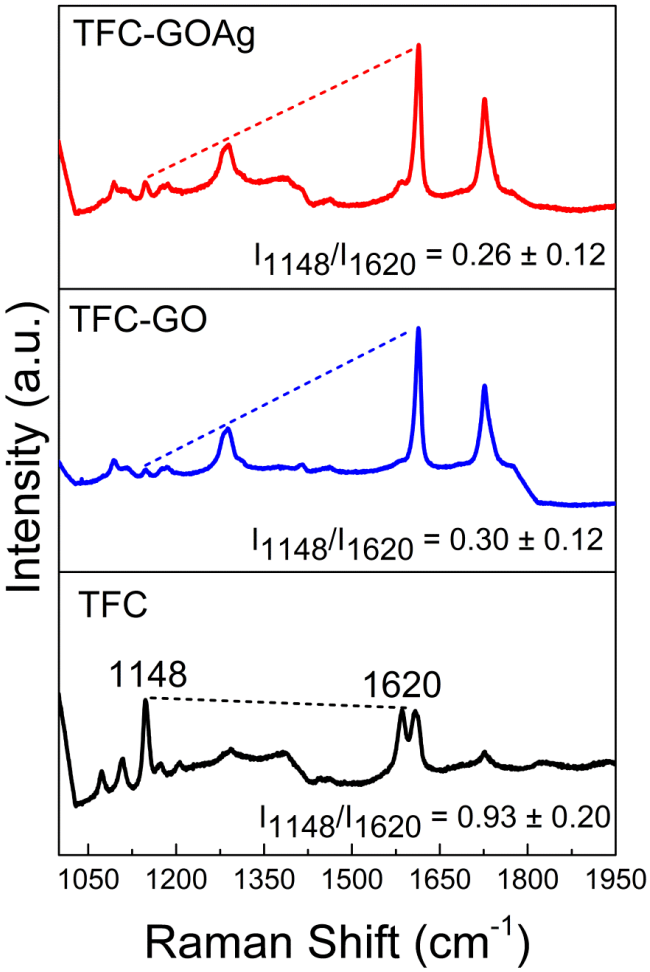

Figure 5: Raman spectra of the TFC (black), TFC-GO (blue), and TFC-GOAg (red) membranes. The ratio between the intensity of the bands at 1148 and 1620 cm^{-1} was used to identify the presence of GO and GOAg on the membrane surface. The I_{1148}/I_{1620} average values are a result of at least five random measurements at different locations on each membrane surface.

3.3 GO and GOAg sheets impact membrane surface properties

AFM images (**Figure 6**) were taken to evaluate changes in the polyamide roughness after modification with GO or GOAg. A significant decrease in surface roughness was observed for TFC-GO as compared to pristine TFC membranes. On the other hand, in comparison with the unmodified control, TFC-GOAg membranes presented only a slight decrease in roughness. The covering of the polyamide ridge-and-valley features by GO sheets might be the cause of the reduction in surface roughness observed for TFC-GO membranes [15]. TFC, TFC-GO, and TFC-GOAg membranes presented a root mean squared (*Rq*) surface roughness of 84.8 ± 5.3, 49.7 ± 6.5, and 77.9 ± 6.2 nm, respectively (**Figure 7A**). This result may suggest that GOAg sheets provided a less effective coating of the membrane surface. It is likely that GO sheets are partially reduced in contact with the reducing agent during the synthesis of GOAg. As a result, GOAg nanocomposite dispersions are less stable and aggregate, which could lead to a decreased diffusion rate of the GOAg sheets towards the membrane surface during modification. As a consequence, the binding of GOAg sheets is probably minimized in comparison to that expected for pristine GO sheets. Furthermore, the AgNPs themselves, especially the aggregates, could increase the roughness for TFC-GOAg compared to TFC-GO membranes.

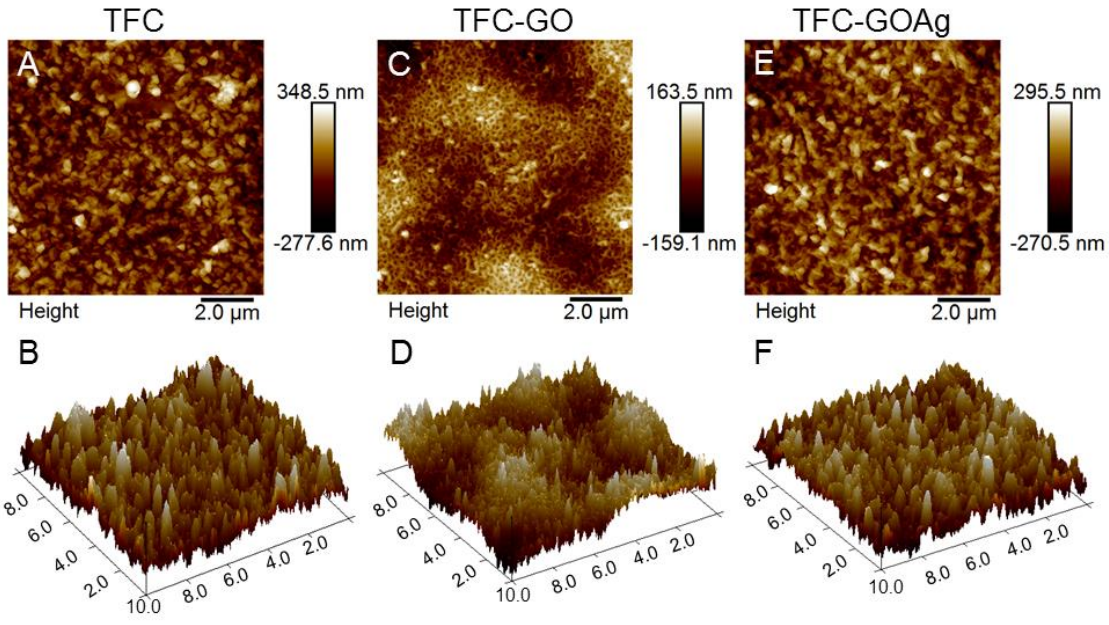

Figure 6: Atomic force microscopy (AFM) images of (A, B) pristine TFC, (C, D) TFC-GO, and (E, F) TFC-GOAg membranes. The units are in micrometers (µm).

Changes in surface hydrophilicity were investigated through static water contact angle measurements (**Figure S2)**. However, no significant differences in contact angle were noticed after functionalization of TFC membranes with either GO (32.6 ± 2.8°) or GOAg sheets (33.8 ± 6.2°), despite the large amount of hydrophilic, oxygen-containing functional groups on the graphene sheets. One reason for this observation is the already relatively very low contact angle of the pristine TFC membranes (38.1 ± 1.9°).

3.4 Functionalization with GOAg nanocomposites does not affect membrane transport properties

One of the greatest challenges of modifying the surface of TFC membranes is to ensure that water permeability (*A*) and salt selectivity (*B*) are not affected by the binding of polymeric molecules or nanomaterials. **Figure 7B** summarizes the *A*, *B*, and *S* parameters for TFC, TFC-GO, and TFC-GOAg membranes. We observed that the *A* and *B* coefficients did not significantly change with the binding of GO or GOAg to the membrane surface ($p > 0.05$), even though TFC-GOAg presented a small decrease in the water permeability coefficient *A* compared to the unmodified membrane (**Figure 7B**). The salt permeability coefficient *B* slightly increased from 1.33 ± 0.21 L m^{-2} h^{-1} for the pristine membrane to 1.64 ± 0.32 and 1.59 ± 0.21 L m^{-2} h^{-1} for TFC-GO and TFC-GOAg membranes, respectively. As expected, **Figure 7B** also reveals that the membrane structural parameter *S* of the pristine TFC membrane did not change by our modification procedure. These results indicate that the functionalization with GO or GOAg does not impact the transport properties of the membrane polyamide layer. This result is consistent with our previous work, where the modification of RO TFC membranes with pristine GO did not change the membrane transport properties [16, 41]. Similar observations have also been reported for TFC RO membranes modified with multiple layers of GO sheets [42]. This low impact of GO on the membrane performance is probably due to its atomic thickness and hydrophilic nature. **Table S1** presents one full set of experimental data (measured water and reverse salt fluxes and relevant coefficients of determination, R^2) for the TFC, TFC-GO, and TFC-GOAg membranes, used for the calculation of *A*, *B*, and *S*.

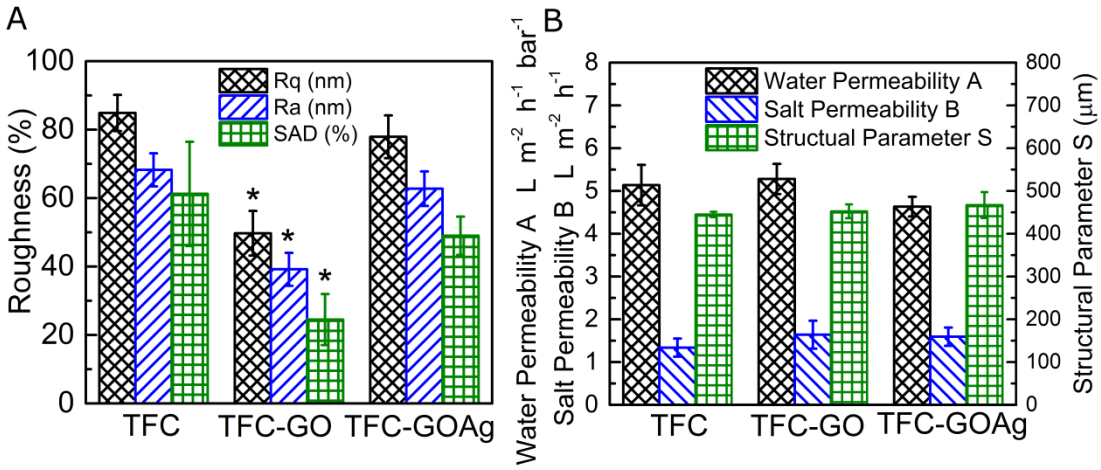

Figure 7: (A) Surface roughness determined by atomic force microscopy (AFM) for pristine TFC, TFC-GO, and TFC-GOAg membranes. The roughness parameters extracted from AFM images are root-mean-square value (Rq), average roughness (Ra), and percent surface area difference (SAD %). The roughness data were collected from at least five different areas on the membrane surface. (B) Transport and performance properties of TFC, TC-GO, and TFC-GOAg membranes: water permeability coefficient *A*, salt (NaCl) permeability coefficient *B*, and structural parameter *S*. Asterisks above bars indicate that the TFC-GO membrane roughness parameters were significantly different ($p < 0.01$) than the corresponding values of the other two membranes.

3.5 Bacterial attachment and viability are significantly suppressed by GOAg

Antimicrobial activity was first evaluated after exposing the membrane surface to *P. aeruginosa* cells for three hours. In comparison to pristine TFC, the TFC-GO membrane displayed no toxic effect towards *P. aeruginosa* (**Figure 8A**). TFC-GOAg membrane, on the other hand, exhibited a bacterial inactivation rate of around 80% against *P. aeruginosa*, relative to the non-modified TFC membranes. In other words, the number of viable cells on TFC-GOAg was significantly lower than that of the unmodified control, implying that functionalization with GOAg imparted a strong antimicrobial activity to the membrane surface.

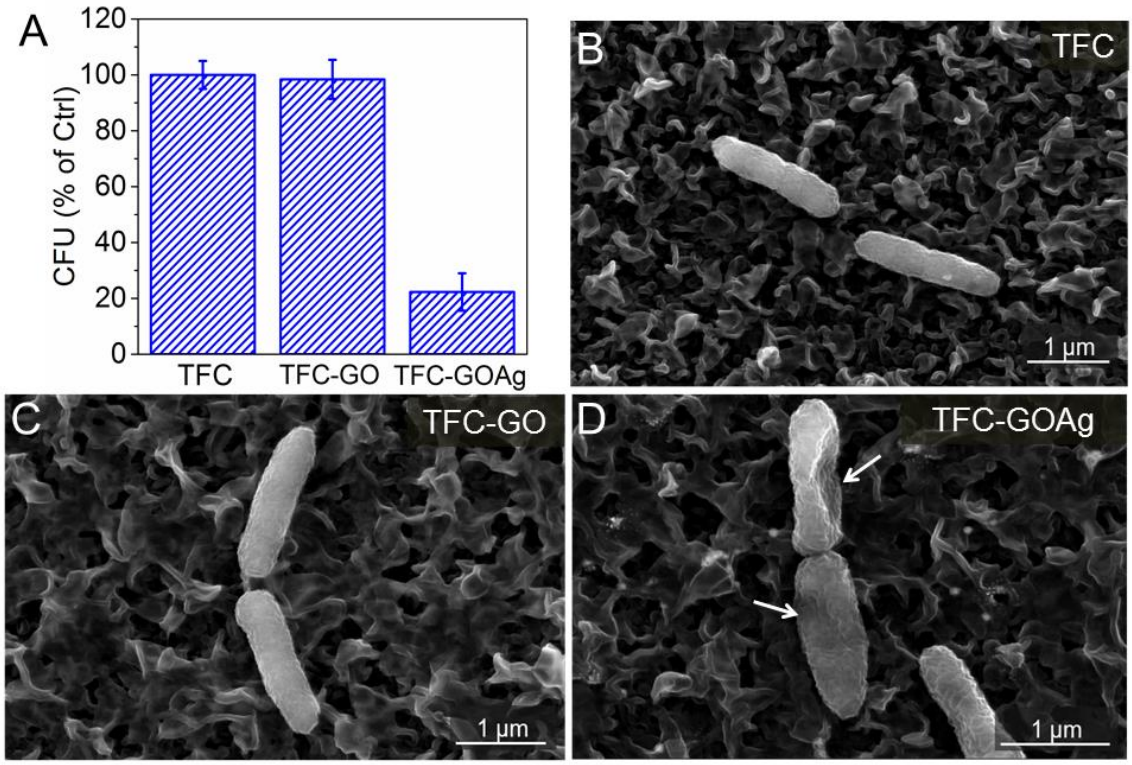

Figure 8: (A) Viable cells of *P. aeruginosa* after three hour contact with the surface of pristine and graphene modified membranes. The viability of *P. aeruginosa* cells is expressed as the percentage of colony-forming units (CFU) relative to the pristine TFC control membrane. Standard deviation error bars were calculated from three independent replicates. Scanning electron microscopy (SEM) images of bacteria cells attached to the polyamide active layer of (B) pristine TFC, (C) TFC-GO, and (D) TFC-GOAg membranes. Severe morphological damage for bacteria cells on TFC-GOAg is highlighted by white arrows on the image (panel D). SEM images were taken at an accelerating voltage of 10 kV.

Morphological characteristics of adhered bacterial cells were examined by SEM (**Figures 8B, C, and D**). The microbial cells attached to pristine TFC membrane remained intact after exposure. However, SEM images clearly demonstrated that *P. aeruginosa* cells on TFC-GOAg membrane surface were severely damaged, as indicated by white arrows in **Figure 8D**. Upon contact with TFC-GOAg surface, the adhered cells revealed a flattened and shrunken morphology. The loss in morphological integrity is likely caused by the presence of AgNPs, and the mechanism of toxicity can be explained by both release of toxic Ag^{+} ions and direct contact with the AgNPs on the membrane surface [25, 43]. The high affinity of silver for thiol (-SH) functional groups of proteins may damage the stability and architecture of the bacterial cell wall through the generation of holes and vacancies [44, 45]. Disruption of cell wall structure could irreversibly affect the transport of nutrients, thus inactivating the bacterial cells.

3.6 GOAg nanocomposite functionalized membranes exhibit reduced biofouling rate.

The anti-biofouling properties of TCF and TFC-GOAg membranes were investigated by allowing *P. aeruginosa* cells to grow on the membrane surface for 24 hours in a dynamic cross-flow biofouling test. One of the consequences of biofilm formation on TFC membranes is the decrease in permeate water flux. As shown in **Figure 9A**, the development of biofilm on pristine TFC membrane resulted in a flux decline of approximately 50%. However, when TFC membrane is functionalized with GOAg nanocomposites, the flux decline is significantly reduced. The difference in the water flux behavior is attributable to differences in the structure and composition of the biofilms on the pristine TFC and TFC-GOAg membranes.

To obtain information about the biofilm properties, the biofouled membranes were characterized by confocal microscopy. **Figures 9 B and D** show representative CLSM images of the biofilm prior and after the functionalization of TFC membranes with GOAg nanosheets, respectively. Dead cells, represented in red color, are more abundant on TFC-GOAg (**Figure 9D**) than on TFC-GO or pristine TFC membranes (**Figures 9B and C**). The dead cell region reached the top layer of the biofilm on the TFC-GOAg membrane, indicating that direct contact with the GOAg nanocomposite was not required and that silver ions could leach and diffuse to the upper cell layers. Therefore, the addition of Ag in a GOAg nanocomposite played a key role in mitigating biofilm development on TFC membranes.

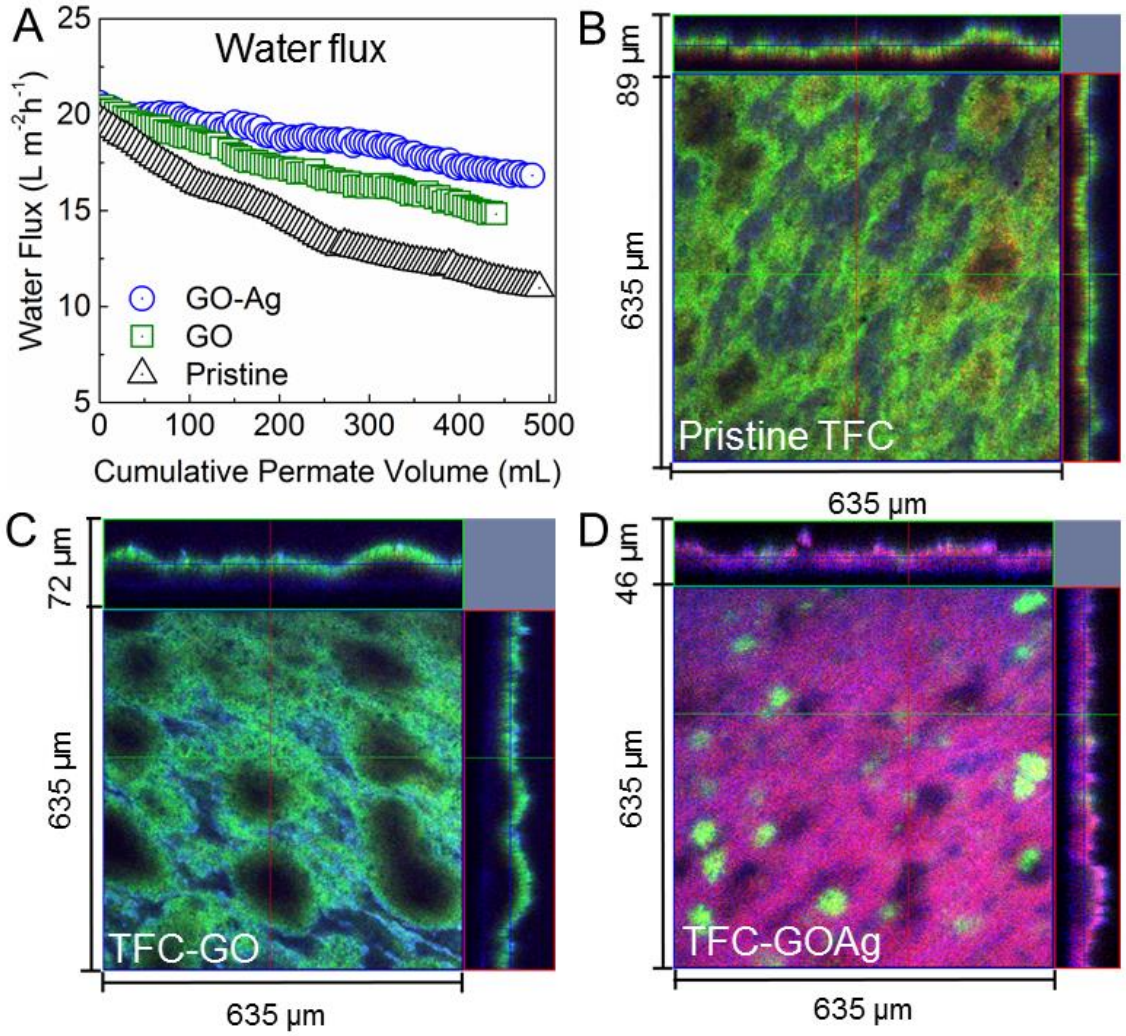

538

539 **Figure 9**: (A) Water flux decline caused by the formation of biofilm during biofouling
540 experiments in a cross-flow cell. Water flux decline data were obtained from two independent
541 duplicates. The biofouling experiments were conducted using synthetic wastewater with
542 glucose as a carbon source. Temperature and cross-flow velocities were kept at 25°C and 9.56
543 cm s^{-1}, respectively. To achieve the initial water flux of 20 L m^{-2} h^{-1}, we used NaCl draw
544 solution in the range of 0.4 to 0.7 M. Under these conditions, the reverse salt fluxes for pristine
545 TFC, TFC-GO, and TFC-GOAg membranes were 110, 115, and 145 mmol·m^{-2}·h^{-1},
546 respectively. Confocal laser scanning microscopy (CLSM) images of *P. aeruginosa* biofilm
547 developed on the polyamide active layer of (B) pristine TFC, (C) TFC-GO, and (D) TFC-
548 GOAg membranes. The biofilm was grown after 24-hour biofouling runs as described in (A).
549 Live cells, dead cells, and exopolysaccharides were stained with Syto 9 (green), propidium
550 iodide (red), and Con A (blue) dyes, respectively.

551

552 **Table 1** summarizes the biofilm properties for TFC, TFC-GO, and TFC-GOAg
553 membranes. For instance, the biofilm on TFC-GOAg membrane was almost two times thinner
554 than that on the pristine TFC membrane. Furthermore, the live cell biovolume (µm^3 µm^{-2}) on
555 TFC-GOAg was decreased by almost 50% compared to the non-modified TFC membrane. The

556 lack of antimicrobial activity for TFC-GO membrane is explained by the relatively large size
557 of the GO sheets [28]. The results observed from confocal imaging are in accordance with the
558 CFU counts reported in Figure 8A, where pristine TFC and TFC-GO membranes exhibited
559 similar antimicrobial properties. The biofilm contents of protein and total carbon were also
560 drastically reduced after modification of TFC membranes with GOAg nanocomposites. The
561 total protein mass was diminished from 18.7 ± 2.5 to 9.1 ± 6.2 pg μm^{-2} after binding GOAg
562 sheets to the membrane surface (**Table 1**).

563 Our findings suggest that bacterial growth on the TFC membrane surface was strongly
564 inhibited by GOAg nanocomposites. The decrease in the number of live cells on the TFC-
565 GOAg membrane led to a significant reduction in biofilm thickness, live cell biovolume, and
566 EPS production (**Table 1**). Our results demonstrate that the development of anti-biofouling
567 TFC membranes can benefit from the physicochemical and biological properties of GOAg
568 nanocomposites. Recognizing that the antimicrobial activity of GOAg nanocomposites is
569 partially dependent on the release of Ag^+ ions, their anti-biofouling properties can be improved
570 by maximizing membrane coverage and/or by tuning the size, shape, and content of AgNPs in
571 the GOAg nanocomposites.

572

Table 1: Characteristics of *P. aeruginosa* biofilm grown on pristine TFC, TFC-GO, and TFC-GOAg membranes after 24 hours. All parameters were determined from confocal laser scanning microscopy (CLSM) images.

Operating condition	Average biofilm thickness (μm) [a]	"Live" cell biovolume ($\mu m^3\ \mu m^{-2}$)	"Dead" cell biovolume ($\mu m^3\ \mu m^{-2}$)	EPS biovolume ($\mu m^3\ \mu m^{-2}$)	Total protein mass (pg μm^{-2})[b]	TOC biomass (pg μm^{-2}) [b]
Pristine TFC	89 ± 5	21.2 ± 4.1	12.1 ± 2.3	20.9 ± 2.2	18.7 ± 2.5	1.57 ± 0.05
TFC-GO	72 ± 2	27.2 ± 5.1	12.1 ± 2.3	12.3 ± 3.6	12.1 ± 4.5	1.11 ± 0.03
TFC-GOAg	46 ± 3	12.5 ± 5.1	29.6 ± 1.1	8.3 ± 3.6	9.1 ± 6.2	0.82 ± 0.07

[a] biofilm thickness and biovolume were averaged, with standard deviations calculated from ten random samples in duplicated experiments.

[b] TOC and protein biomasses were presented with standard deviations calculated from four measurements by two membrane coupons.

4. Conclusion

In this study, we report the synthesis of GOAg nanocomposites and their further application as antimicrobial agents for the control of biofouling in forward osmosis membranes. GOAg nanocomposites were prepared through a straightforward process whereby silver nanoparticles are in-situ nucleated on GO sheets. The formation of silver nanoparticles on GO sheets is done by using glucose as a reducing agent. The resulting GOAg nanocomposites displayed silver nanoparticles with an average size of 16 nm which were bound irreversibly on the GO surface. Carboxylic groups on GOAg were used as target points to bind the graphene sheets to the amine-terminated polyamide layer. The surface modification of TFC membranes with GO or GOAg nanocomposites was successfully demonstrated by SEM and Raman spectroscopy analyses. We also show that the intrinsic transport properties of TFC membranes were not affected by the modification with GO or GOAg nanocomposites.

Static antimicrobial assays showed that GOAg modified membranes were able to significantly inhibit the attachment of *Pseudomonas aeruginosa* cells. Unlike some previous studies, the membrane modified just with GO showed no toxicity to bacterial cells. In addition, dynamic biofouling experiments performed using a bench-scale FO system demonstrated the anti-biofouling property of membranes modified with GOAg sheets. A massive amount of dead cells can be seen on the confocal images taken from TFC-GOAg membranes. In addition, the biovolume of live cells was substantially decreased for membranes modified with GOAg. Dynamic biofouling experiments also showed that the flux decline due to biofouling development was reduced by 30% after modification of TFC membranes with GOAg nanocomposites. Our results suggest that membrane functionalization with GOAg is a robust platform to yield TFC membranes possessing enhanced biofouling resistance.

5. Acknowledgment

A.F.F thanks the Program “Science without Borders” through the Brazilian Council of Science and Technology for their financial support. F.P. acknowledges financial support from the Natural Sciences and Engineering Research Council of Canada postdoctoral fellowship. The authors thank Dr. Zhenting Jiang and Dr. Jennifer Girard for their support on the SEM and Raman analyses, respectively. Additionally, the authors also

acknowledge the Yale Institute of Nanoscale and Quantum Engineering (YINQE) and Dr. Michael Rooks for their support on the TEM analyses.

6. REFERENCES

[1] M. Elimelech, W.A. Phillip, The Future of Seawater Desalination: Energy, Technology, and the Environment, Science, 333 (2011) 712-717.
[2] M.A. Shannon, P.W. Bohn, M. Elimelech, J.G. Georgiadis, B.J. Marinas, A.M. Mayes, Science and technology for water purification in the coming decades, Nature, 452 (2008) 301-310.
[3] R.J. Petersen, Composite reverse osmosis and nanofiltration membranes, Journal of Membrane Science, 83 (1993) 81-150.
[4] N.Y. Yip, A. Tiraferri, W.A. Phillip, J.D. Schiffman, M. Elimelech, High Performance Thin-Film Composite Forward Osmosis Membrane, Environmental Science & Technology, 44 (2010) 3812-3818.
[5] J.S. Baker, L.Y. Dudley, Biofouling in membrane systems — A review, Desalination, 118 (1998) 81-89.
[6] M. Herzberg, M. Elimelech, Biofouling of reverse osmosis membranes: Role of biofilm-enhanced osmotic pressure, Journal of Membrane Science, 295 (2007) 11-20.
[7] E. Bar-Zeev, U. Passow, S. Romero-Vargas Castrillón, M. Elimelech, Transparent Exopolymer Particles: From Aquatic Environments and Engineered Systems to Membrane Biofouling, Environmental Science & Technology, 49 (2015) 691-707.
[8] G.-D. Kang, C.-J. Gao, W.-D. Chen, X.-M. Jie, Y.-M. Cao, Q. Yuan, Study on hypochlorite degradation of aromatic polyamide reverse osmosis membrane, Journal of Membrane Science, 300 (2007) 165-171.
[9] G. Ye, J. Lee, F. Perreault, M. Elimelech, Controlled Architecture of Dual-Functional Block Copolymer Brushes on Thin-Film Composite Membranes for Integrated "Defending" and "Attacking" Strategies against Biofouling, ACS applied materials & interfaces, 7 (2015) 23069-23079.
[10] D. Saeki, S. Nagao, I. Sawada, Y. Ohmukai, T. Maruyama, H. Matsuyama, Development of antibacterial polyamide reverse osmosis membrane modified with a covalently immobilized enzyme, Journal of Membrane Science, 428 (2013) 403-409.
[11] M. Ben-Sasson, X. Lu, E. Bar-Zeev, K.R. Zodrow, S. Nejati, G. Qi, E.P. Giannelis, M. Elimelech, In situ formation of silver nanoparticles on thin-film composite reverse osmosis membranes for biofouling mitigation, Water research, 62 (2014) 260-270.
[12] J. Yin, Y. Yang, Z. Hu, B. Deng, Attachment of silver nanoparticles (AgNPs) onto thin-film composite (TFC) membranes through covalent bonding to reduce membrane biofouling, Journal of Membrane Science, 441 (2013) 73-82.
[13] M. Ben-Sasson, K.R. Zodrow, Q. Genggeng, Y. Kang, E.P. Giannelis, M. Elimelech, Surface Functionalization of Thin-Film Composite Membranes with Copper Nanoparticles for Antimicrobial Surface Properties, Environmental science & technology, 48 (2014) 384-393.
[14] S. Kang, M.S. Mauter, M. Elimelech, Microbial Cytotoxicity of Carbon-Based Nanomaterials: Implications for River Water and Wastewater Effluent, Environmental Science & Technology, 43 (2009) 2648-2653.
[15] A. Tiraferri, C.D. Vecitis, M. Elimelech, Covalent Binding of Single-Walled Carbon Nanotubes to Polyamide Membranes for Antimicrobial Surface Properties, ACS Applied Materials & Interfaces, 3 (2011) 2869-2877.
[16] F. Perreault, M.E. Tousley, M. Elimelech, Thin-Film Composite Polyamide Membranes Functionalized with Biocidal Graphene Oxide Nanosheets, Environmental Science & Technology Letters, 1 (2014) 71-76.

[17] H.S. Lee, S.J. Im, J.H. Kim, H.J. Kim, J.P. Kim, B.R. Min, Polyamide thin-film nanofiltration membranes containing TiO2 nanoparticles, Desalination, 219 (2008) 48-56.
[18] M. Hu, B. Mi, Enabling Graphene Oxide Nanosheets as Water Separation Membranes, Environmental science & technology, 47 (2013) 3715-3723.
[19] K.S. Novoselov, A.K. Geim, S.V. Morozov, D. Jiang, Y. Zhang, S.V. Dubonos, I.V. Grigorieva, A.A. Firsov, Electric Field Effect in Atomically Thin Carbon Films, Science, 306 (2004) 666-669.
[20] D.R. Dreyer, S. Park, C.W. Bielawski, R.S. Ruoff, The chemistry of graphene oxide, Chemical Society Reviews, 39 (2010) 228-240.
[21] F. Perreault, A. Fonseca de Faria, M. Elimelech, Environmental applications of graphene-based nanomaterials, Chemical Society Reviews, 44 (2015) 5861-5896.
[22] Y. Zhu, S. Murali, W. Cai, X. Li, J.W. Suk, J.R. Potts, R.S. Ruoff, Graphene and Graphene Oxide: Synthesis, Properties, and Applications, Advanced Materials, 22 (2010) 3906-3924.
[23] A.F. de Faria, D.S.T. Martinez, S.M.M. Meira, A.C.M. de Moraes, A. Brandelli, A.G.S. Filho, O.L. Alves, Anti-adhesion and antibacterial activity of silver nanoparticles supported on graphene oxide sheets, Colloids and Surfaces B: Biointerfaces, 113 (2014) 115-124.
[24] E.S. Orth, J.E.S. Fonsaca, S.H. Domingues, H. Mehl, M.M. Oliveira, A.J.G. Zarbin, Targeted thiolation of graphene oxide and its utilization as precursor for graphene/silver nanoparticles composites, Carbon, 61 (2013) 543-550.
[25] A.F. de Faria, F. Perreault, E. Shaulsky, L.H. Arias Chavez, M. Elimelech, Antimicrobial Electrospun Biopolymer Nanofiber Mats Functionalized with Graphene Oxide–Silver Nanocomposites, ACS applied materials & interfaces, 7 (2015) 12751-12759.
[26] W.S. Hummers, R.E. Offeman, Preparation of Graphitic Oxide, Journal of the American Chemical Society, 80 (1958) 1339-1339.
[27] V.C. Tung, M.J. Allen, Y. Yang, R.B. Kaner, High-throughput solution processing of large-scale graphene, Nat Nano, 4 (2009) 25-29.
[28] F. Perreault, A.F. de Faria, S. Nejati, M. Elimelech, Antimicrobial Properties of Graphene Oxide Nanosheets: Why Size Matters, ACS Nano, 9 (2015) 7226-7236.
[29] Y. Yin, Z.-Y. Li, Z. Zhong, B. Gates, Y. Xia, S. Venkateswaran, Synthesis and characterization of stable aqueous dispersions of silver nanoparticles through the Tollens process, Journal of Materials Chemistry, 12 (2002) 522-527.
[30] A. Tiraferri, N.Y. Yip, A.P. Straub, S. Romero-Vargas Castrillon, M. Elimelech, A method for the simultaneous determination of transport and structural parameters of forward osmosis membranes, Journal of Membrane Science, 444 (2013) 523-538.
[31] M. Xie, E. Bar-Zeev, S.M. Hashmi, L.D. Nghiem, M. Elimelech, Role of Reverse Divalent Cation Diffusion in Forward Osmosis Biofouling, Environmental Science & Technology, 49 (2015) 13222-13229.
[32] S. Liu, M. Hu, T.H. Zeng, R. Wu, R. Jiang, J. Wei, L. Wang, J. Kong, Y. Chen, Lateral Dimension-Dependent Antibacterial Activity of Graphene Oxide Sheets, Langmuir, 28 (2012) 12364-12372.
[33] A. Panáček, M. Kolář, R. Večeřová, R. Prucek, J. Soukupová, V. Kryštof, P. Hamal, R. Zbořil, L. Kvítek, Antifungal activity of silver nanoparticles against Candida spp, Biomaterials, 30 (2009) 6333-6340.
[34] L. Liu, J. Liu, Y. Wang, X. Yan, D.D. Sun, Facile synthesis of monodispersed silver nanoparticles on graphene oxide sheets with enhanced antibacterial activity, New Journal of Chemistry, 35 (2011) 1418-1423.

Thin-film composite forward osmosis membranes functionalized with graphene oxide–silver nanocomposites for biofouling control

Supplementary Data

Journal of Membrane Science

Andreia F. Faria[1], Caihong Liu[1,2], Ming Xie[1,3], Francois Perreault[1,4], Long D. Nghiem[5], Jun Ma[2], and Menachem Elimelech [1*]

[1]*Department of Chemical and Environmental Engineering, Yale University, New Haven, Connecticut 06520-8286, USA*

[2] *State Key Laboratory of Urban Water Resource and Environment, Harbin Institute of Technology, Harbin 150090, China*

[3]*Institute for Sustainability and Innovation, College of Engineering and Science, Victoria University, PO Box 14428, Melbourne, Victoria 8001, Australia*

[4]*School of Sustainable Engineering and the Built Environment, Arizona State University, Tempe, AZ, 85287-3005.*

[5] *Water Infrastructure Laboratory, School of Civil, Mining and Environmental Engineering, University of Wollongong, Wollongong, NSW 2522, Australia*

* Corresponding author: Menachem Elimelech, Email: menachem.elimelech@yale.edu, Phone: (203) 432-2789

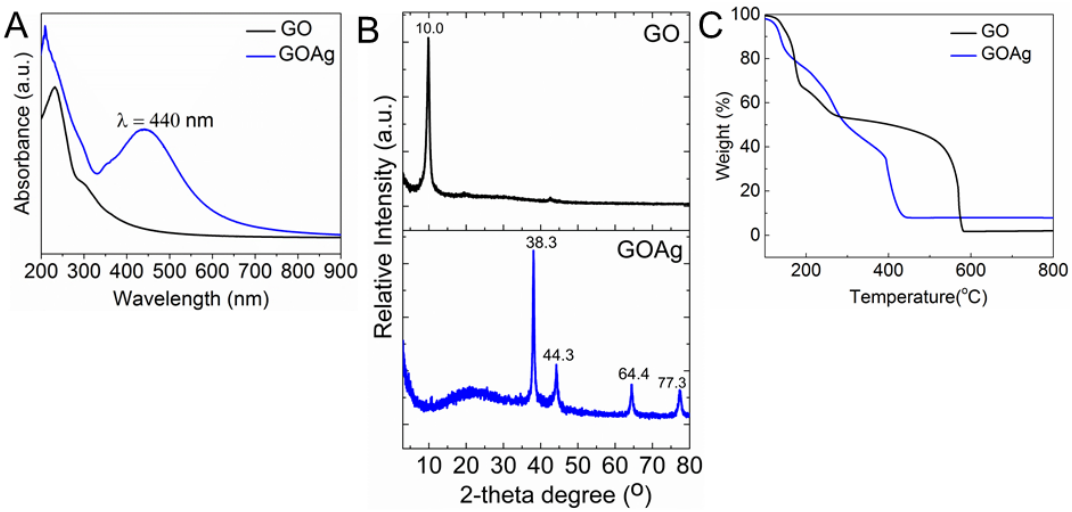

Figure S1: (A) UV-Vis spectra of GO and GOAg suspensions (100 µg mL^{-1}). The presence of plasmonic band at 440 nm suggests the formation of GOAg nanocomposite. (B) XRD spectra of GO and GOAg. The 2θ peaks at 38.3, 44.3, 64.4, and 77.3 are related to the crystalline planes of silver nanoparticles. (C) Thermogravimetric curves (TGA) of GO and GOAg shows their loss of weight at high temperatures. The residues above 600°C can be associated with the content of silver in the GOAg sample.

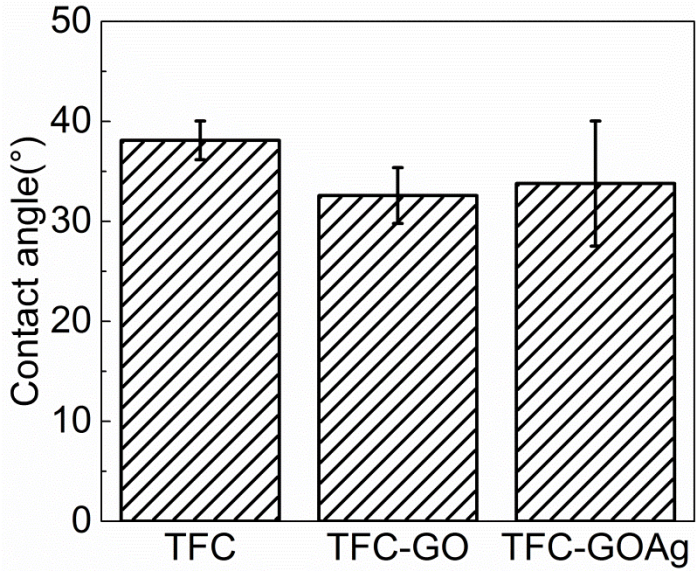

Figure S2: Water contact angle for unmodified TFC, TFC-GO, and TFC-GOAg membranes.

Table S1: Estimation of water and salt permeability coefficients of TFC, TFC-GO, and TFC-GOAg membranes by the FO four-step characterization method [1]. The final water permeability coefficient *A*, salt permeability coefficient *B*, and structural parameter *S* presented in the manuscript were determined from three sets of independent measurements for each membrane.

Membrane	Step	J_w ($Lm^{-2}h^{-1}$)	J_s ($mmolm^{-2}h^{-1}$)	J_w/J_s ($Lmmol^{-1}$)	R^2-J_w	R^2-J_s
TFC	i	12.42	81.2	0.19	0.988	0.985
	ii	17.35	104.1	0.197		
	iii	20.47	128.6	0.209		
	iv	25.72	155.18	0.219		
TFC-GO	i	13.66	78.8	0.173	0.997	0.998
	ii	18.03	104.8	0.172		
	iii	23.06	129.8	0.178		
	iv	27.68	155.14	0.178		
TFC-GOAg	i	12.42	81.2	0.153	0.989	0.994
	ii	17.35	104.1	0.167		
	iii	20.47	128.6	0.159		
	iv	25.72	155.18	0.166		

Reference:

[1] A. Tiraferri, N.Y. Yip, A.P. Straub, S. Romero-Vargas Castrillon, M. Elimelech, A method for the simultaneous determination of transport and structural parameters of forward osmosis membranes, Journal of Membrane Science, 444 (2013) 523-538.

[35] J. Tang, Q. Chen, L. Xu, S. Zhang, L. Feng, L. Cheng, H. Xu, Z. Liu, R. Peng, Graphene Oxide–Silver Nanocomposite As a Highly Effective Antibacterial Agent with Species-Specific Mechanisms, ACS Applied Materials & Interfaces, 5 (2013) 3867-3874.
[36] J. Li, C.-y. Liu, Ag/Graphene Heterostructures: Synthesis, Characterization and Optical Properties, European Journal of Inorganic Chemistry, 2010 (2010) 1244-1248.
[37] C. Li, X. Wang, F. Chen, C. Zhang, X. Zhi, K. Wang, D. Cui, The antifungal activity of graphene oxide–silver nanocomposites, Biomaterials, 34 (2013) 3882-3890.
[38] T.S. Sreeprasad, S.M. Maliyekkal, K.P. Lisha, T. Pradeep, Reduced graphene oxide–metal/metal oxide composites: Facile synthesis and application in water purification, Journal of Hazardous Materials, 186 (2011) 921-931.
[39] H.J. Kim, A.E. Fouda, K. Jonasson, In situ study on kinetic behavior during asymmetric membrane formation via phase inversion process using Raman spectroscopy, Journal of Applied Polymer Science, 75 (2000) 135-141.
[40] L.M. Malard, M.A. Pimenta, G. Dresselhaus, M.S. Dresselhaus, Raman spectroscopy in graphene, Physics Reports, 473 (2009) 51-87.
[41] F. Perreault, H. Jaramillo, M. Xie, M. Ude, L.D. Nghiem, M. Elimelech, Biofouling Mitigation in Forward Osmosis Using Graphene Oxide Functionalized Thin-Film Composite Membranes, Environmental Science & Technology, 50 (2016) 5840-5848.
[42] W. Choi, J. Choi, J. Bang, J.-H. Lee, Layer-by-Layer Assembly of Graphene Oxide Nanosheets on Polyamide Membranes for Durable Reverse-Osmosis Applications, ACS Applied Materials & Interfaces, 5 (2013) 12510-12519.
[43] M.S. Mauter, Y. Wang, K.C. Okemgbo, C.O. Osuji, E.P. Giannelis, M. Elimelech, Antifouling Ultrafiltration Membranes via Post-Fabrication Grafting of Biocidal Nanomaterials, ACS Applied Materials & Interfaces, 3 (2011) 2861-2868.
[44] M. Rai, A. Yadav, A. Gade, Silver nanoparticles as a new generation of antimicrobials, Biotechnology Advances, 27 (2009) 76-83.
[45] I. Sondi, B. Salopek-Sondi, Silver nanoparticles as antimicrobial agent: a case study on E. coli as a model for Gram-negative bacteria, Journal of Colloid and Interface Science, 275 (2004) 177-182.